

# Parallel Simulation of Atmospheric Gas Dispersion

S.S. Beauchemin, Q. Brandon, M. Kotb, H.O. Hamshari, and M.A. Bauer  
Department of Computer Science  
The University of Western Ontario  
London ON N6A 5B7

## ***Abstract***

*Events such as atmospheric gas dispersion by industrial accidents or processes are generally predicted with Gaussian plumes, coupled with local models of gas emission. In this contribution we investigate the association of integral models of instantaneous emission with Gaussian dispersion processes, for predicting the progression of potentially hazardous low-altitude emissions over sensitive or populated areas. In particular, we develop an approach which accounts for dynamic wind by means of gas plume fragmentation and parallel estimation of gas dispersion.*

## **1 Introduction**

Because of its simplicity, the Gaussian dispersion model is often used for predicting the progression of atmospheric gas plumes [1, 4, 8]. This model relies on a number of hypotheses to determine the path and spread of plumes, the most fundamental stating that the dispersion must be *passive*, which is equivalent to considering the gas density as roughly the same as that of the surrounding atmosphere.

Before reaching the stage of passive dispersion, initial conditions of gas emissions are often addressed differently, as various gases may have densities differing from ambient air (depending on molecular weight, temperature, altitude of emission, and so on). Failing to consider such parameters in the early stages could result in considerable prediction errors, either in concentration levels or geographical spread.

The use of Gaussian dispersion models require that terrain be free of significant obstacles such as skyscrapers or mountain ranges, or that the altitude of the emission source be sufficiently high to ignore obstacles. Other hypotheses include the absence of atmospheric turbulence, and gas densities

which minimize the effect of gravity on the plume. Under such conditions, the dispersion results are usually considered correct from approximately 100 meters from the emitting source and beyond [2].

Hence, in our low-altitude emission framework, the sole use of a Gaussian dispersion model is clearly inadequate. A local emission model for the source is required, and we adopt the integral model as an instantaneous emission source, providing the initial conditions for the Gaussian dispersion simulation. An additional hypothesis pertaining to the integral model requires that gas dispersion be relatively significant, generally in the order of a few  $m^3s^{-1}$ . A gas cloud following an integral model evolves at very small spatio-temporal scales when compared with the much larger dispersion scales inherent to a Gaussian model. However, the integral model is required, if only to provide the dispersion process with adequately realistic initial parameters.

The integral model employs a stack of cylinders, describing volumes (or *puffs*) containing gas particles. These puffs are updated through an iterative process until they reach the density of surrounding air. Ultimately, puffs with such densities are injected in the stack of the Gaussian model, for large-scale dispersion computations to begin.

To combine the integral and Gaussian models while preserving a relative flexibility, we choose an approach in which both models share common environmental parameters, operating over a discretized grid map describing dynamic atmospheric and terrain conditions. At each iteration, the combined model updates the environmental conditions and the characteristics of emission sources, and injects gas puffs in the integral or Gaussian model. Results are expressed as concentration and dispersion grids over the region of interest.

## 2 The Integral Model

Once a dense gas is emitted, it enters a gravity flow stage where it collapses under its own weight for a period of time, until the ensuing entrainment of air (and possibly heating by solar radiation) dilutes the gas sufficiently to enter a passive dispersion stage. At this point the cloud forms a layer which is in contact with the ground. Air flow then becomes the dominant factor involved in the dispersion of the cloud. The gravity flow stage for an instantaneous gas emission is generally modeled with a vertical gas cylinder whose properties, such as the atmospheric entrainment of air it creates, dimension, temperature, volume, and density may be estimated over time with the integral model.

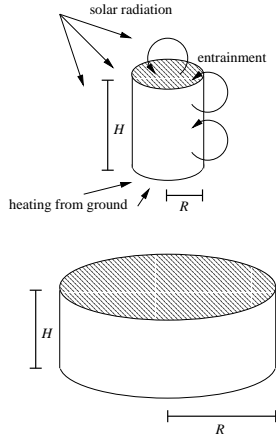


Figure 1: *Collapse of gas cylinder under various environmental and gravitational effects.*

The radius of the cylinder corresponding to the instantaneous emission is expected to grow, as the gas cloud collapses under gravity. As this process takes place, the difference between the air and the gas densities diminishes to reach a point in time when the radius of the cylinder becomes stable [9] (at  $\rho = \rho_a$ )<sup>1</sup>:

$$R' = K \sqrt{gH \frac{\rho - \rho_a}{\rho_a}} \quad (1)$$

The total mass of air entrained by the gas cloud, which significantly contributes to its dilution,

<sup>1</sup>A complete description of the variables and their units is given in Appendix A.

evolves in time at a rate given by:

$$M'_a = \pi \rho_a \left( R' 2\alpha_1 H R + R'^2 \alpha_2 \frac{U_t}{R_1} \right) \quad (2)$$

The entrainment of air is a function of the areas of the edge and top of the cylinder, as well as the speed of turbulent air.

The temperature of the cloud is influenced by various factors, the most significant being the temperature of the ground ( $Q_1$ ) with which the gas is in contact with, and the temperature of the surrounding air ( $Q_2$ ):

$$T' = \frac{Q_1 + Q_2'}{M_a C_a + M_g C_g} \quad (3)$$

It is assumed that turbulent convection is the means by which heat is supplied to the gas from the ground:

$$Q_1 = \alpha_3 (T - T_s)^{\frac{4}{3}} \quad (4)$$

The heat transfer between the air and the cloud is expressed as:

$$Q_2' = M'_a C_a (T_a - T) \quad (5)$$

From previous equations, we can derive the volume, height, mean concentration and density of the cloud:

$$V = \frac{M_a + M_g}{\rho} \quad (6)$$

$$H = \pi \frac{V}{R^2} \quad (7)$$

$$C = \frac{M_g}{V} \quad (8)$$

$$\rho = T(M_a + M_g) T_a^{-1} \left( \frac{M_a}{\rho_a} + \frac{M_g}{\rho_g} \right)^{-1} \quad (9)$$

The integral model is adequately suited for dense gas dispersions until the difference in gas and air densities becomes negligible. At this point, the model provides the initial parameters to a passive dispersion calculation, such as that carried out by a Gaussian model.

## 3 The Gaussian Model

The simplest form of atmospheric dispersion is passive. Nonetheless, determining the standard deviations for the Gaussian model in realistic cases

WIND	SOLAR RADIATION ( $W m^{-2}$ )			
$m s^{-1}$	$\geq 925$	925-675	675-175	$\leq 175$
$< 2$	A	A	B	D
2 – 3	A	B	C	D
3 – 5	B	B	C	D
5 – 6	C	C	D	D
$> 6$	C	D	D	D

Table 1: Daytime atmospheric stability class as a function of wind and solar radiation.

WIND	CLOUD COVER (in %)	
$m s^{-1}$	$\geq 50$	$< 50$
$< 2$	F	F
2 – 3	E	F
3 – 5	D	E
$> 5$	D	D

Table 2: Nighttime atmospheric stability class as a function of wind and cloud cover.

remains a complex and experimental problem. According to Pasquill’s experiments [5, 6], the initial standard deviations  $\sigma_y$  and  $\sigma_z$  (the crosswind and the vertical dispersion coefficients<sup>2</sup>, respectively) for the Gaussian model can be computed as:

$$\sigma_y \text{ or } \sigma_z = ax^b + c \quad (10)$$

where  $x$ , the distance from the source, is expressed in  $km$ . Values for parameters  $a$ ,  $b$ , and  $c$  are obtained from Tables 3 and 4, according to six atmospheric stability classes, from A (very unstable) to F (very stable). The values of these parameters differ whether  $\sigma_y$  or  $\sigma_z$  is computed. Atmospheric stability depends on factors such as wind speed, incident solar radiation, cloud cover, and possibly ground roughness at low altitudes. Tables 1 and 2 give the atmospheric stability class as a function of wind and solar radiation for daytime and as a function of wind and cloud cover for nighttime.

Once  $\sigma_x$ ,  $\sigma_y$ , and  $\sigma_z$  are computed and the simulation is ongoing, concentrations may be estimated at a given time step with the following Gaussian:

$$C = \frac{M}{(2\pi)^{\frac{3}{2}} \det S} \times \exp \left\{ -\frac{1}{2} [S^{-1}(\mathbf{x} - \mathbf{x}_c)]^T S^{-1}(\mathbf{x} - \mathbf{x}_c) \right\} \quad (11)$$

<sup>2</sup>Pasquill assumed  $\sigma_x = \sigma_y$ , which is a reasonable hypothesis for crosswind dispersion.

$x \leq 1km$				
CLASS	$\sigma$	$a$	$b$	$c$
A	$\sigma_y$	0.215	0.858	0.00
	$\sigma_z$	0.467	1.890	0.01
B	$\sigma_y$	0.155	0.889	0.00
	$\sigma_z$	0.103	1.110	0.00
C	$\sigma_y$	0.105	0.903	0.00
	$\sigma_z$	0.066	0.915	0.00
D	$\sigma_y$	0.068	0.908	0.00
	$\sigma_z$	0.032	0.822	0.00
E	$\sigma_y$	0.050	0.914	0.00
	$\sigma_z$	0.023	0.745	0.00
F	$\sigma_y$	0.034	0.908	0.00
	$\sigma_z$	0.014	0.727	0.00

Table 3: Standard deviations according to Pasquill’s atmospheric stability classes, for passive dispersions under 1 km [6].

where

$$S = \begin{pmatrix} \sigma_x & 0 & 0 \\ 0 & \sigma_y & 0 \\ 0 & 0 & \sigma_z \end{pmatrix}$$

is the matrix of dispersion coefficients. Concentration is obtained at  $\mathbf{x} = (x, y, z)^T$  while the center of the Gaussian is located at  $\mathbf{x}_c = (x_c, y_c, z_c)^T$ . As the wind pushes the Gaussian cloud, its center is updated with the prevailing wind velocity vector  $\mathbf{u}$ . In addition, the distance  $x$  from the source to the center of the Gaussian cloud is recomputed as<sup>3</sup>:

$$x = \left( \frac{\sigma_x - c}{a} \right)^{\frac{1}{b}} \quad (12)$$

This description of the Gaussian model accounts for one instantaneous emission of gas only. A source emitting in a continuous fashion must be modeled differently. The instantaneous integral and Gaussian models can be extended to include series of instantaneous emissions over time, each emission at time  $t_i$  possessing its own mass of gas  $M_i$ . Hence, in order to simulate a continuous emission, the integral model is fitted with a gas cylinder stack while the Gaussian model receives a puff stack. Each new emission is placed in the gas cylinder stack, where the simulation begins. When a cylinder has reached relative stability, its parameters are fed into the puff stack of the Gaussian

<sup>3</sup>The initial dispersion coefficients for the Gaussian are provided by the integral model after the gas cylinder has collapsed. Hence, the position of the source is said to be virtual, as it does not reflect the position of the gas cylinder.

$x > 1km$				
CLASS	$\sigma$	$a$	$b$	$c$
E	$\sigma_y$	0.050	0.914	0.00
	$\sigma_z$	0.148	0.015	-1.126
F	$\sigma_y$	0.034	0.908	0.000
	$\sigma_z$	0.031	0.306	-0.017

Table 4: *Standard deviations according to Pasquill’s atmospheric stability classes, for passive dispersions over 1 km [6]. Standard deviations for classes A through D are as per Table 3.*

model, where it is left to develop according to prevailing environmental conditions. The resulting set of instantaneous emissions forms a plume governed by passive dispersion.

These models are obvious simplifications of environmental reality which entails more complex phenomena such as ground reflection, absorption, roughness, and particle fallout [2].

## 4 Puff Fragmentation

The Gaussian model, when used to predict continuous emissions, possesses a relative adaptability as each puff evolves with respect to its local environmental conditions, provided that these are available on such a local scale. Over time, the scale of Gaussian puffs increases to a point where atmospheric conditions within their extent may vary significantly. To account for such variation, an effective approach consists of fragmenting large Gaussian puffs into smaller ones, while preserving the properties of the plume, such as spread and concentration. The original Gaussian puff prior to the fragmentation is represented by an elliptical sphere. We use a hexagonal sphere packing scheme to create a group of elliptical spheres, each a Gaussian puff with a distribution as close to the original sphere as possible. This fragmentation ensures a minimal number of elliptical spheres with relative positional symmetries. Figure 2 shows such a fragmentation.

This process results in a central puff containing 21.81% of the initial gaseous mass with the remaining 12 puffs containing 6.52% each. The dispersion coefficients  $\sigma_x$ ,  $\sigma_y$ , and  $\sigma_z$  from each of the 13 puffs are set to  $\frac{2}{3}$  of the initial cloud coefficients. Figures 3, 4 and 5 show the positional symmetries of the sphere pack.

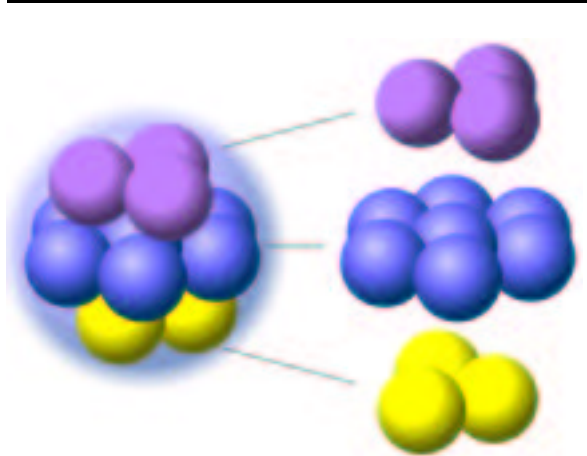


Figure 2: *The fragmentation of a Gaussian puff into smaller puffs. A compact hexagonal packing of 13 Gaussian puffs replaces the original one. The centers and standard deviations of the resulting puffs are chosen to minimize the difference in gas concentration observed within the larger puff.*

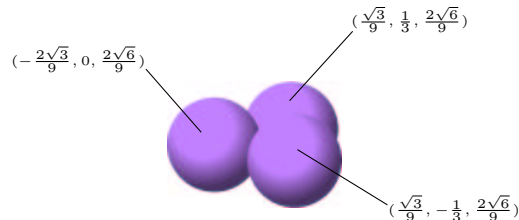


Figure 3: *The positional symmetries of the top layer puffs starting at the bottom center of the initial cloud.*

## 5 Parallelization

From a computational standpoint, the combined integral-Gaussian model with puff fragmentation is demanding, particularly when the number of Gaussian puffs becomes large. Fortunately, the model lends itself rather naturally to parallelization.

A number of observations concerning the characteristics of the combined model can be made: during a simulation, the integral model is in use for what amounts to be a small duration per emitted gas cylinder, owing to rapid collapse and dilution. In comparison, the Gaussian model is computationally costlier, due to the number of Gaussian puffs fed to its stack by the integral model, the duration of each puff (hours, perhaps days), and particu-

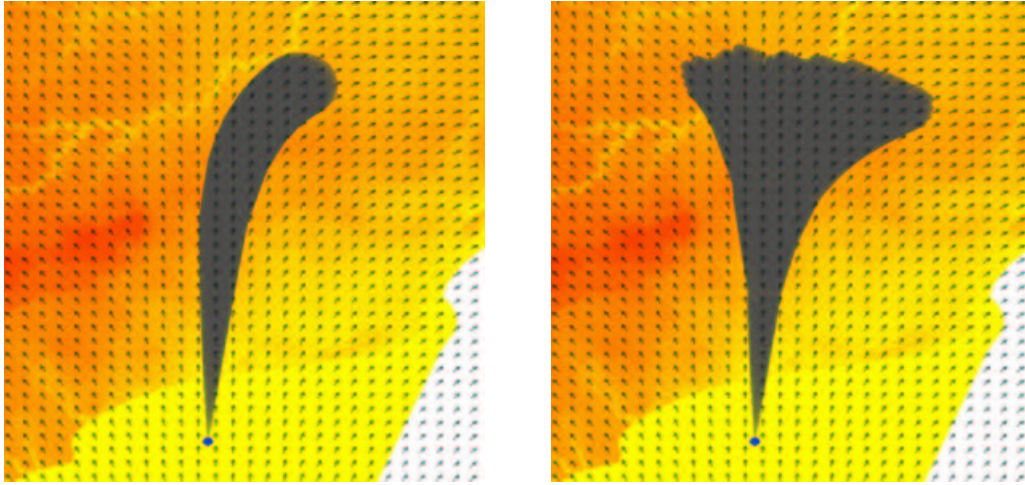


Figure 6: **a) (right):** Classical plume progression from a continuous emission source. **b) (left):** Plume progression with Gaussian puff fragmentation. Different trajectories under identical wind vector fields are experienced.

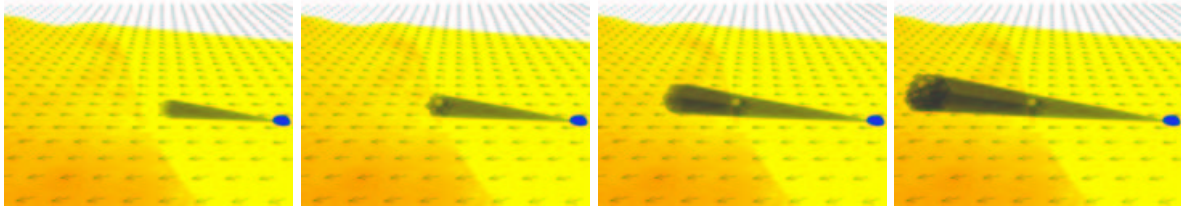


Figure 7: **(from left to right):** A Sequence of images showing the Gaussian puff fragmentation, occurring at puff radii reaching 500 m. **a)** The initial puff progression. **b)** The first fragmentation occurrence. **c)** The progression of the resulting puffs. **d)** The second fragmentation occurrence.

larly the puff fragmentation mechanism, which exponentially increases the number of puffs entering the simulation. In addition, one of the most demanding processes is the calculation of estimated concentrations over grid maps.

Consider a continuous gaseous emission lasting a total time  $T = N_1 t$ , with a Gaussian puff emitted at every  $t$ . The total number of puffs, without fragmentation is thus  $N_1$ . If we assume that each puff is fragmented  $n$  times, then  $N$ , the number of Gaussian puffs in the simulation is:

$$N = N_1 \sum_{i=0}^n P^i \quad (13)$$

where  $P = 12$ . For instance, if 1000 initial puffs are released, after 4 simultaneous fragmentations, the number of puffs in the simulation reaches 22,621,000. In addition, numerous concentration calculations must be carried out for each puff, and the amount of these increases as the extent of the puffs becomes larger. A monoprocessor architecture is clearly inadequate for long simulations such as radiological emissions and volcanic phenomena, which may last for days.

An adequate parallel architecture for the parallelization of the combined integral-Gaussian model is a shared-memory, multiprocessor architecture allowing computing units to share one instance of the

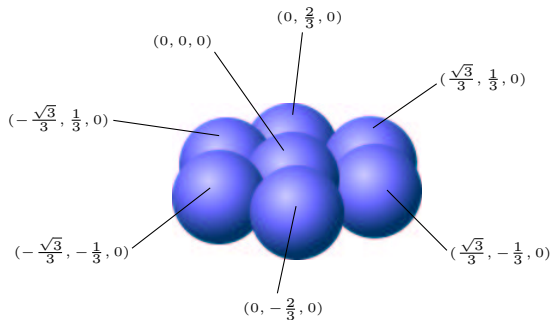


Figure 4: *The positional symmetries of the middle layer puffs starting at the bottom center of the initial cloud.*

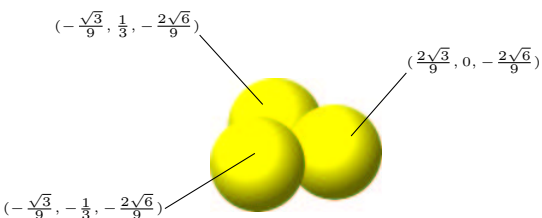


Figure 5: *The positional symmetries of the bottom layer puffs starting at the bottom center of the initial cloud.*

grid map of the region of interest, while ensuring an adequate distribution of the computation of dispersion and concentration. For instance, the puffs could be evenly distributed among available processors in a natural fashion each time they are introduced in the simulation. In the context of the preceding example, a multiprocessor architecture with  $2^{10}$  available computing units would, at the peak of the simulation, reduce the computing load from 22M puffs to 22,091 per processor, which is an acceptable computational burden.

## 6 Experiments

Simulation experiments were conducted over an elevation grid map of the Sarnia region in Canada. Elevation is color-coded from yellow (low elevation) to orange (high elevation). The Gaussian puffs forming the gaseous plumes are displayed

with transparency factors unrelated to concentration, in order to show their position. The extent of the displayed puffs is a fraction of their dispersion coefficients. These experiments are conducted with average atmospheric conditions, for 1.5 to 3 hours of real dispersion time. Wind direction is variable with speed  $\|\mathbf{u}\|_2$  averaging  $1.5 \text{ m s}^{-1}$ . The gas emission  $M_g$  is set to  $0.005 \text{ kg}$  and occurs at every second. The simulation time step  $\delta t$  is set to  $1 \text{ s}$ . A list for the values of the remaining parameters can be found in Appendix B.

The first experiment, shown in Figure 6 demonstrates, under a spatially variable wind vector field, the difference in gaseous progression between the classical integral-Gaussian plume model with and without puff fragmentation. Figure 6a) shows the dispersion results when the extent of puffs becomes sufficiently large to be subjected to more than a single, constant wind vector: the plume deviates toward the dominant wind. However, as shown in Figure 6b), with a puff fragmentation mechanism, the trajectory of the plume is consonant with the variation observed in the wind vector field, resulting in an improvement in accuracy, which still needs to be quantified [7].

The second experiment, shown in Figure 7, is a sequence of images showing the puff fragmentation mechanism. The blue region represents the emission site, simulated with the integral model. In figure 7a) the initial gaseous emission starts with a single Gaussian puff. After a amount of time into the simulation, the largest dispersion coefficient ( $\sigma_x$ ,  $\sigma_y$ , or  $\sigma_z$ ) reaches  $500 \text{ m}$ , and triggers the fragmentation process. The resulting puffs are displayed in Figure 7b). As time elapses, the puffs experience progression and increased extent (Figure 7c)). Ultimately, the fragmentation process is triggered a second time, as depicted in Figure 7d).

## 7 Conclusion

Air dispersion modeling remains an elusively imprecise branch of environmental science [7]. Inherent difficulties are numerous, among which we find the experimental evaluation of various critical parameters, such as Pasquill's dispersion coefficients [6], or the mathematical complexities involved with modeling turbulent phenomena.

We proposed a combined integral-Gaussian atmospheric dispersion model including a mechanism for the fragmentation of gas puffs. The immediate

benefits of this model reside in the qualitative improvement in concentration and spread predictions, at an increased computational cost, which may be alleviated with an adequate parallel implementation on shared-memory, massively parallel computing equipment.

Improvements to this model include the quantification of the gain in dispersion modeling accuracy, the inclusion of light gases, and adequate model corrections for terrains with significant slopes and obstacles, in the case of dense gas emissions.

## References

- [1] M. Benarie. *Urban Air Pollution Modeling*. MIT Press, Cambridge, Mass., 1980.
- [2] European Process Safety Center. *Atmospheric Dispersion*. Institution of Chemical Engineers, 1999.
- [3] F.A. Gifford and S.R. Hanna. Urban air pollution modeling. In *Conf. of Int. Union of Air. Poll. Prev. Assoc.*, Washington, DC, 1970.
- [4] R. MacDonald. Theory and objectives of air dispersion modeling. University of Waterloo, Internal Report, 2003.
- [5] F. Pasquill. The estimation of dispersion of wind-borne material. *Meteorology Magazine*, 90:33–49, 1961.
- [6] F. Pasquill and F.B. Smith. *Atmospheric Diffusion*. Ellis Horwood Series in Environmental Science. Chichester, West Sussex, 3rd edition, 1983.
- [7] J.S. Touma, W.M. Cox, H. Thistle, and J.G. Zapert. Performance evaluation of dense gas dispersion models. *Journal of Applied Meteorology*, 34(3):603–615, 1994.
- [8] D.B. Turner. *Workbook of Atmospheric Dispersion Estimates: An Introduction to Air Dispersion Modeling*. CRC Press, 2nd edition, 1994.
- [9] A.R. Van Ulden. Simple estimates for vertical diffusion from sources near the ground. *Atmospheric Environment*, 12:2125–2129, 1978.

## A Notation

This section provides definitions and units for parameters used in the combined integral-Gaussian model.

$C$	: gas concentration ( $kg\ m^3$ )
$C_a$	: specific heat of air ( $kg\ J\ K^{-1}$ )
$C_g$	: specific heat of gas ( $kg\ J\ K^{-1}$ )
$H$	: height of gas cylinder ( $m$ )
$K$	: Van Ulden's parameter ( $m$ )
$M$	: mass of pollutant ( $kg$ )
$M_a$	: air entrained by cylinder ( $kg$ )
$M_g$	: mass of gas in cylinder ( $kg$ )
$Q_1$	: heating by the ground ( $J$ )
$Q_2$	: heating by the air ( $J$ )
$R$	: radius of gas cylinder ( $m$ )
$R_1$	: Richardson's number
$T$	: gas temperature ( $K$ )
$T_a$	: air temperature ( $K$ )
$T_s$	: ground temperature ( $K$ )
$U_t$	: horiz. turbulent air speed ( $m\ s^{-1}$ )
$V$	: cylinder volume ( $m^3$ )
$g$	: gravity ( $m\ s^{-2}$ )
$\alpha_1$	: air entrainment by cylinder edge
$\alpha_2$	: air entrainment by cylinder top
$\alpha_3$	: gas thermal conductivity ( $J\ K^{\frac{3}{4}}$ )
$\rho$	: average cylinder density ( $kg\ m^{-3}$ )
$\rho_a$	: air density ( $kg\ m^{-3}$ )
$\mathbf{u}$	: $(u, v)^T$ wind velocity ( $m\ s^{-1}$ )
$\mathbf{x}$	: $(x, y, z)^T$ point of concentration
$\mathbf{x}_c$	: $(x_c, y_c, z_c)^T$ Gaussian center

## B Experimental Values

$C_a$	: 1000 $J\ kg^{-1}\ K^{-1}$
$C_g$	: 2400 $J\ kg^{-1}\ K^{-1}$
$K$	: 1
$M_a$	: 0.4 $kg$
$R_1$	: 1
$T$	: 300 $K$
$T_a$	: 295 $K$
$T_s$	: 293 $K$
$U_t$	: 1 $m\ s^{-1}$
$g$	: 9.81 $N\ kg^{-1}$
$\rho_a$	: 1.184 $kg\ m^{-3}$
$\rho_g$	: 2.4 $kg\ m^{-3}$